remote sensing

MDPI

Article

Remote Sensing-Based Biomass Assessment of *Hedysarum coronarium* from Multispectral UAV Imagery in a Mediterranean Pasture

Nicola Furnitto [1], Sabina I. G. Failla [1,*], Giuseppe Sottosanti [1], Marcella Avondo [1], Matteo Bognanno [2], Luisa Biondi [1] and Juan Miguel Ramírez-Cuesta [3]

[1] Department of Agriculture, Food and Environment, University of Catania, Via S. Sofia 100, 95123 Catania, Italy; nicola.furnitto@phd.unict.it (N.F.); peppesottosanti99@gmail.com (G.S.); marcella.avondo@unict.it (M.A.); luisa.biondi@unict.it (L.B.)
[2] Department of Agriculture, University of Reggio Calabria, Via Dell'università 25, 89124 Reggio Calabria, Italy; matteo.bognanno@unirc.it
[3] Department of Ecology and Global Change, Desertification Research Centre (CIDE, CSIC-UV-GV), Moncada, 46113 Valencia, Spain; jm.ramirez.cuesta@csic.es
* Correspondence: sabina.failla@unict.it

Highlights

What are the main findings?

- UAV-based multispectral vegetation indices accurately estimated fresh and dry above-ground biomass in the Mediterranean "Sulla" pasture.
- Visible-band greenness indices were among the best-performing predictors of biomass.

What are the implications of the main findings?

- Inter-sensor harmonization enabled the combined analysis of data collected in two different growing seasons.
- A simple single-index workflow may support grazing management through rapid and non-destructive biomass assessment.

Abstract

The accurate estimation of pasture above-ground biomass (AGB) is critical for optimizing stocking rates and ensuring the sustainable use of Mediterranean pastures. This study developed empirical models to estimate fresh (AGB_{fresh}) and dry above-ground biomass (AGB_{dry}) using multispectral imagery acquired by Unmanned Aerial Vehicles (UAVs) in a *Hedysarum coronarium* pasture in Sicily, Italy. Field biomass was destructively sampled simultaneously with UAV surveys in 28 georeferenced plots during pre- and post-grazing phases over the 2023–2024 and 2024–2025 seasons. Data were collected with a DJI Mavic 3 Multispectral (for the 2024 test) and a DJI Matrice 300 + Altum-PT (for the 2025 test) and radiometrically calibrated to surface reflectance. Because two different multispectral sensors were used across years, an inter-sensor harmonization step was applied before vegetation-index calculation. Thirty-three vegetation indices were extracted as mean values within circular buffers of 1 m radius, centered on each sample plot to accommodate GNSS/georeferencing uncertainty. For each vegetation index, linear and exponential models were calibrated using 66% of the dataset and validated on the remaining 33% to predict fresh and dry above-ground biomass, and model performance was assessed using R^2 and RMSE. On the validation dataset, ARVI2 and EVI2 showed the highest explanatory power for AGB_{fresh} (R^2 = 0.89), with ARVI2 providing the lower RMSE (2047 g m^{-2}). For AGB_{dry}, visible-band indices such as NGRDI and GRVI were among the best performers,

Academic Editor: Kun Jia

Received: 26 March 2026
Revised: 11 May 2026
Accepted: 12 May 2026
Published: 16 May 2026

reaching R^2 = 0.85 with RMSE = 1371 g m^{-2}. Visible-band greenness indices were among the most competitive predictors, whereas several conventional NIR-based indices showed only moderate performance. Overall, this UAV-based multispectral approach represents a promising and interpretable tool for biomass estimation in heterogeneous Mediterranean pastures, although further validation across additional seasons and sites is required to strengthen its transferability.

Keywords: pasture; grassland monitoring; biomass estimation; vegetation indices; vegetation analysis; empirical modeling

1. Introduction

Grasslands are a major terrestrial biome—covering ~25% of the global land area—and provide essential ecosystem services, including forage provision, carbon sequestration, biodiversity support, water regulation, and soil protection [1–3]. In the Mediterranean, especially in semi-arid interiors such as the Sicilian hinterland, grasslands also sustain extensive livestock systems and contribute to the socio-ecological resilience of rural communities [4–6].

Productivity in Mediterranean pastures is highly variable and shaped by climate variability, grazing management (stocking rates, timing, spatial patterns), and soil fertility [7,8]. Reliable estimates of available herbaceous biomass—dry and fresh above-ground biomass (AGB_{dry} and AGB_{fresh}, respectively)—are therefore crucial to optimize grazing pressure, prevent overgrazing or undergrazing, improve farm planning, and support agro-environmental policies [9,10]. The two biomass definitions were considered complementary in this study. AGB_{fresh} is more closely related to the immediately available forage mass and is influenced by plant water content, whereas AGB_{dry} provides a more stable estimate of structural biomass. Evaluating both variables, therefore, allows a more complete assessment of pasture condition and helps to determine whether UAV-derived vegetation indices respond differently to water-related versus structural biomass components. Traditional destructive sampling is accurate but labour-intensive and costly, limiting frequent or large-scale monitoring [11,12].

Remote sensing (RS) offers a scalable alternative to destructive sampling by providing repeated observations of vegetation status over time. In this context, the growing availability of high-revisit CubeSat constellations (e.g., PlanetScope Dove and SuperDove) is further expanding precision-agriculture applications by enabling frequent multispectral monitoring at fine spatial and temporal scales [13,14]. In grassland and pasture systems, satellite platforms (e.g., Sentinel-1/2 and Landsat) have been widely used to estimate biomass and related biophysical variables across broad areas and seasons, often coupled with statistical or machine-learning approaches to improve predictive performance [15–17]. However, satellite-based monitoring can be limited at the farm scale by pixel size and cloud constraints, particularly when pastures are heterogeneous, and grazing effects occur in fine-grained patches. In these contexts, Unmanned Aerial Vehicles (UAVs) complement satellite observations by enabling flexible acquisition timing and centimeter-level spatial detail, which is especially valuable for supporting field-scale decisions in managed grazing systems [18].

Recent advances in UAV multispectral imagery allow detailed observation of vegetation, capturing fine spatial variability relevant to pasture dynamics [19–23]. Vegetation indices such as NDVI, EVI/EVI2, NDRE, and SAVI are widely used for herbaceous biomass estimation, although index saturation under dense vegetation cover remains a known challenge, partly mitigated by red-edge-based or soil-adjusted formulations [24–30].

Beyond purely spectral indices, UAV-based structural information derived from photogrammetry (e.g., canopy surface models and height metrics) has also proved useful for non-destructive biomass estimation in swards and pasture plots [31–33]. In several grassland applications, combining structural metrics with spectral predictors can improve robustness across phenological stages and management conditions. Nevertheless, the added processing steps and the dependence on stable image geometry and surface reconstruction may reduce simplicity and transferability in routine monitoring. For operational adoption, there is therefore continued interest in compact multispectral workflows based on interpretable indices and low-complexity empirical relationships.

Despite these advances, semi-arid Mediterranean pastures under rotational grazing remain comparatively under-represented in the literature, even though they are common in regional livestock systems and exhibit distinctive phenology, strong within-field heterogeneity, and climate sensitivity [5,6,9,34]. In addition, Mediterranean pastures are strongly constrained by interannual climate variability, with rainfall-driven pulses of growth and rapid shifts in vegetation structure that can alter the spectral–biomass relationship across years. This reinforces the need to test model stability under variable seasonal conditions [18,35]. Moreover, while modern machine-learning approaches can achieve high accuracy, they often demand large training datasets and yield models that are harder to interpret and transfer to farm-level decisions. Such models may also remain strongly site-specific and may not generalize well to areas with different vegetation composition, soil background, or environmental conditions than those used for calibration. In production settings, there is a clear need for simple, transparent empirical models that can be replicated with routine UAV flights and modest data requirements [10,36].

In this study, we investigated whether a UAV-based multispectral approach, relying on single vegetation indices and simple empirical regressions, can provide reliable estimates of fresh and dry above-ground biomass (AGBfresh and AGBdry) in a semi-arid Mediterranean pasture of *Hedysarum coronarium* ("Sulla") managed under rotational grazing. Specifically, the study aimed to: (i) assess the strength of the relationships between field-measured biomass and a broad set of UAV-derived vegetation indices; (ii) identify the most robust indices for biomass estimation across contrasting pre- and post-grazing conditions and across two growing seasons; and (iii) evaluate whether a simple and interpretable modelling framework may offer an operational alternative for fine-scale pasture monitoring under heterogeneous Mediterranean conditions. Rather than maximizing model complexity, our objective was to test the practical usefulness and transferability of a low-complexity and interpretable workflow that could be replicated with routine UAV acquisitions and limited data requirements. In this context, more advanced approaches based on multiple predictors, structural metrics, or machine-learning algorithms may provide additional predictive gains, but they also require more complex processing chains, larger calibration datasets, and may be less straightforward to interpret in operational applications.

2. Materials and Methods

2.1. The Experimental Site

The study was conducted in a 0.7-hectare pasture dominated by *Hedysarum coronarium* L. ("Sulla") near Villarosa (province of Enna), Sicily, Italy (37°37′43.7″N, 14°11′02.0″E) (Figure 1). The pasture consisted of a 2–3-year-old stand of *Hedysarum coronarium* L. estab-

lished by seeding at 100 kg ha^{-1}. The sward also included a small amount of spontaneous herbaceous species typical of Sicilian Mediterranean grasslands (e.g., *Pulicaria vulgaris*, *Echium italicum* subsp. *italicum*, *Dittrichia viscosa*, and *Cirsium spinosissimum*).

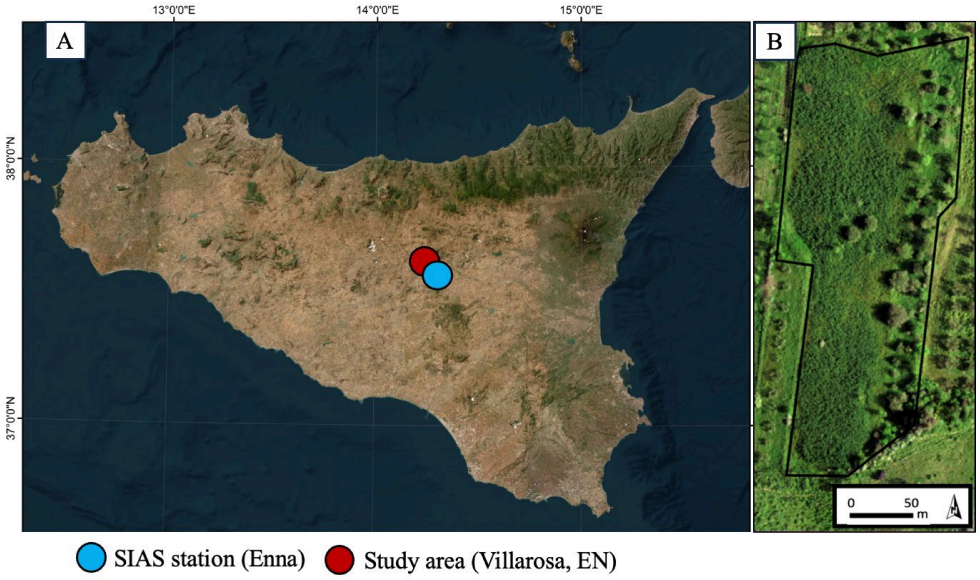

Figure 1. (**A**) Location of the study area near Villarosa (Enna province, Sicily, southern Italy; 37.628851, 14.183906) and of the SIAS weather station in Enna used for meteorological data (37.566223, 14.260471). (**B**) High-resolution UAV orthomosaic of the *Hedysarum coronarium* pasture (0.7 ha) acquired on 15 May 2025 at the study site.

The soils are predominantly clayey, with high water-holding capacity and low infiltration, which can lead to temporary waterlogging after rainfall and pronounced drying during summer drought [37]. The site is located between 500 and 580 m above sea level, with slopes that locally influence the water balance and the development of AGB.

The study area is characterized by a semi-arid Mediterranean climate, with rainfall mainly occurring in autumn–winter and a marked summer drought [38]. Meteorological data (air temperature and precipitation) were obtained from the SIAS (Sistema Informativo Agrometeorologico Siciliano) weather station in Enna, located ~8 km from the study site (straight-line distance).

The pasture was managed under rotational grazing with a flock of 150 Valle del Belice sheep (adult ewes $\geq$ 2 years old; individual live weight 45–60 kg). Ewes were lactating during the grazing period, and animal category/physiological stage and grazing management were kept consistent across years. Grazing was conducted in spring for 10 consecutive days, with animals allowed to graze for 90 min day^{-1}, typically from 08:00 to 09:30, to contain grazing pressure, promote regrowth, and limit overgrazing. Stocking rate and grazing schedule were maintained consistently across both years.

2.2. Biomass Sampling and Processing

Four field campaigns were carried out in May and June 2024 and 2025, corresponding to pre-grazing (20 May 2024 and 15 May 2025) and post-grazing (7 June 2024 and 3 June 2025) conditions. On each field date, the UAV survey and the destructive biomass sampling were performed in immediate succession to ensure close temporal correspondence between remotely sensed and ground-measured data. UAV imagery was acquired immediately before biomass harvesting. At each sampling date, biomass was collected at 28 georeferenced locations and based on 1 m^2.

Quadrat positions were centered on permanent field markers and georeferenced using a Stonex S850P GNSS receiver (WGS84; horizontal accuracy ± 0.50 m) (STONEX Srl, Milano, Italy). This procedure ensured reliable relocation of sampling points across monitoring dates and supported the UAV–ground linkage described in Section 2.3.

Immediately after harvesting, the AGB_{fresh} of each quadrat (n = 28 per campaign) was weighed in the field. Samples were then oven-dried at 60 °C until constant weight (approximately 60 h) to determine AGB_{dry}.

The resulting ground dataset was used to calibrate and validate the empirical biomass models based on UAV-derived vegetation indices.

2.3. Data Acquisition

In the year 2024, flights were carried out using a DJI Mavic 3 Multispectral (SZ DJI Technology Co., Ltd., Shenzhen, in Guangdong province, China), equipped with an integrated multispectral camera. In the second year (2025), surveys were conducted with a DJI Matrice 300, with an Altum PT camera on board that combines high-resolution multispectral sensors and a thermal sensor (Table 1). These two UAV imaging systems were used following an upgrade in the imaging platform, while a calibration was carried out to preserve spectral comparability between datasets.

Table 1. Characteristics of the imaging systems used in 2024 and 2025 (B: blue; G: green; R: red; RE: red edge; NIR: near-infrared; MS: multispectral; PAN: panchromatic; LWIR: long-wave infrared).

Platform	Sensor	Multispectral Bands	Thermal
DJI Mavic 3 Multispectral	Integrated multispectral camera	G (560 ± 16 nm); R (650 ± 16 nm); RE (730 ± 16 nm); NIR (860 ± 26 nm)	(-)
DJI Matrice 300	AgEagle/MicaSense Altum-PT (MS + PAN + LWIR)	B (475 ± 32 nm); G (560 ± 27 nm); R (668 ± 14 nm); RE (717 ± 12 nm); NIR (842 ± 57 nm)	LWIR (7.5–13.5 µm)

For biomass modelling, only VIS–NIR reflectance bands (common to both systems) were considered in the present study. Radiometric calibration—reflectance panel and downwelling light sensor (DLS)—and flight altitude were kept consistent across missions to minimize sensor-related bias.

To further reduce platform-related differences between years, an inter-sensor harmonization step was applied between the DJI Mavic 3 Multispectral and the MicaSense Altum-PT data. This harmonization was based on two additional UAV flights conducted over the same experimental area on the same day and within a short time interval. A total of 1000 points were randomly selected across the study area, and mean reflectance values were extracted using a 1 m buffer around each point to reduce the effect of minor georeferencing and co-registration mismatches between orthomosaics. A global linear relationship between M3M- and Altum-PT-derived reflectance values was then used to harmonize DJI Mavic 3 Multispectral reflectance to the Altum-PT reference scale before vegetation indices were calculated. The corresponding calibration plot is reported in the Supplementary Material (Figure S1).

Multispectral imagery was acquired on the same dates as field biomass sampling and immediately before destructive harvesting, in order to ensure temporal consistency between UAV-derived spectral data and ground measurements. Flights were planned at a constant altitude of 50 m Above Ground Level (AGL), providing ultra-high-resolution

coverage of the entire study area (2 cm pixel^{-1}). All flights were conducted between 11:30 and 12:30 (local time) under low-to-moderate wind conditions ($\leq$6 m s^{-1}) to limit platform-induced image blur and ensure stable acquisition. Forward and side overlap were set to 80% and 70%, respectively, to ensure robust photogrammetric reconstruction, and flight speed was set to 2 m s^{-1} to limit motion blur and optimize data quality.

2.4. Data Processing

UAV imagery was processed in Pix4DFields (Pix4D SA, Prilly, Switzerland) to produce radiometrically calibrated, georeferenced multispectral orthomosaics using a reflectance panel and a DLS. Orthorectification was performed via structure-from-motion (SfM), and ground control points (GCPs) ensured accurate co-registration with plot locations. Subsequent spatial processing and spectral data extraction were carried out in ArcGIS Pro ver. 3.4 (Esri, Redlands, CA, USA).

To link UAV observations with field-measured biomass, a systematic extraction around each georeferenced sampling point was applied. For every plot and date, a circular buffer (radius = 1.0 m) was created in ArcGIS. The dimension of the buffer was selected intentionally to better accommodate GNSS and georegistration uncertainty while capturing a reflectance signal representative of the sampled biomass. Within each buffer, mean surface reflectance from the multispectral bands was extracted for the 28 georeferenced locations across the four acquisition dates (pre- and post-grazing in both 2024 and 2025).

Starting from VIS–NIR reflectance (green, red, red-edge, NIR), 33 vegetation indices (VIs) were computed (Table S1). For presentation and interpretation purposes, the calculated vegetation indices were also grouped into functional families according to their spectral formulation and primary intended use, including NIR–red, NIR–green, contrast-based, atmospherically resistant, soil-adjusted, red-edge/chlorophyll, visible-band, water/pigment-stress, and triangular/geometry-based indices [39–69]. For each sampling plot and date, VIs were computed as mean values within circular buffers centered on the quadrat (r = 1.0 m). VI calculations were performed in ArcGIS, and datasets were assembled and quality-checked in Microsoft Excel to ensure consistency across years and phases.

2.5. Statistical Analysis and Biomass Estimation Modeling

The modelling framework was designed to test whether single UAV-derived vegetation indices could provide reliable and operationally simple predictors of AGB in a heterogeneous Mediterranean pasture. For this reason, each vegetation index (VI) was evaluated individually against the two response variables, fresh above-ground biomass (AGB_{fresh}) and dry above-ground biomass (AGB_{dry}), rather than combining multiple predictors within more complex multivariate models. This modelling choice was intended to preserve interpretability, reduce the risk of over-parameterization in relation to dataset size, and facilitate the identification of indices with potential practical applicability in routine UAV-based pasture monitoring.

For each VI, two empirical regression forms were tested: (i) a linear model, $AGB = a + b \cdot VI$, and (ii) an exponential model, $AGB = a \cdot^{(b \cdot VI)}$. The exponential formulation was fitted after log-transformation. Model parameters were estimated by ordinary least squares. Model performance was assessed using a hold-out calibration/validation procedure, in which 66% of the observations were used for calibration and the remaining 33% for independent validation. The same modelling procedure was applied separately for AGB_{fresh} and AGB_{dry}. The modelling dataset consisted of 112 plot-date observations for AGB_{fresh} and 112 for AGB_{dry}, derived from 28 georeferenced plots sampled across four acquisition dates. Under the 66% and 33% hold-out strategy, approximately 74 observations were used for calibration and 38 for independent validation for each response variable.

The distinction between AGB_{fresh} and AGB_{dry} is also relevant for interpretation, as spectral relationships may partly differ depending on the relative influence of vegetation water content versus structural biomass. Predictive performance was quantified for both subsets using the coefficient of determination (R^2) and the root mean square error (RMSE, g m^{-2}). Because each regression model was based on a single vegetation index, the number of fitted parameters remained low, which helped limit over-parameterization relative to more complex multivariate approaches. Model stability was assessed by comparing calibration and independent validation performance across the hold-out split. For each VI, the functional form retained in the results tables corresponds to the model providing the best balance between explained variance and prediction error.

Climate data were not included as predictor variables in the biomass models. Instead, temperature and precipitation data were used as contextual information to interpret seasonal and interannual differences in pasture growth conditions, particularly because the study aimed to assess the predictive value of UAV-derived spectral information alone. Given the limited number of monitoring dates and the strong temporal coupling between climatic conditions and acquisition year/season, including climate variables directly in the regression framework would have introduced an additional source of complexity beyond the scope of the present study.

Differences in ground-measured AGB between the two sampling campaigns within each period (pre- versus post-grazing) were assessed using one-way ANOVA, with statistical significance set at $\alpha = 0.05$, using StataSE software ver. 19.5.

3. Results

3.1. Environmental Conditions and Ground Biomass Variability

Weather conditions during the two monitored seasons (October 2023–September 2025) are summarized in Figure 2 to provide an environmental context for biomass dynamics. Air temperature followed the expected Mediterranean seasonal pattern, with winter minima and summer maxima above 30 °C. Rainfall was concentrated in discrete events, with a marked summer drought in both years. Overall, the 2024–2025 season showed higher rainfall than 2023–2024, especially during the autumn–early spring period.

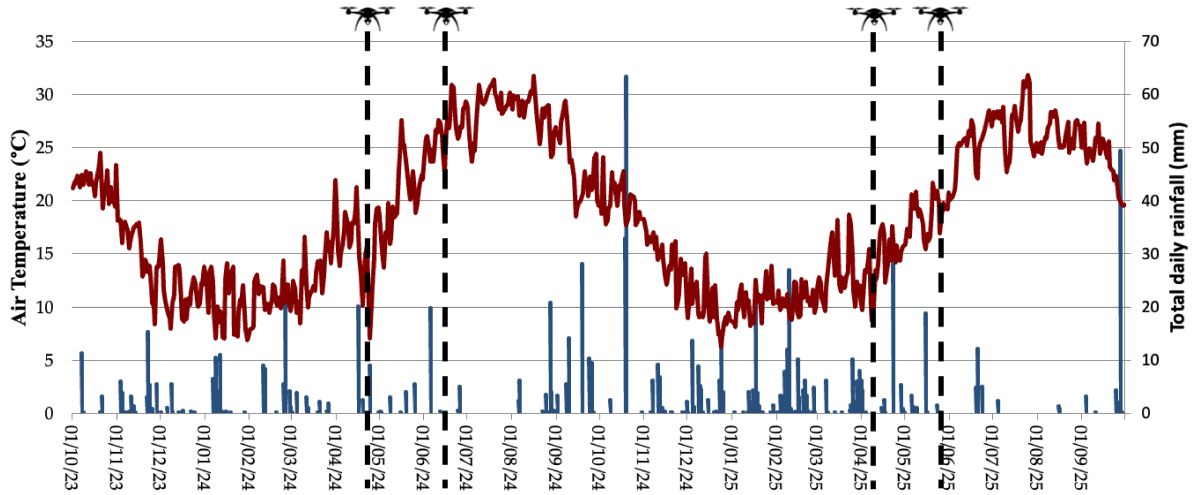

Figure 2. Climate conditions (air temperature and daily rainfall) at the study site during the 2023–2024 and 2024–2025 growing seasons. The flight dates are highlighted.

Ground-measured biomass showed clear differences between years and grazing phases (Figure 3). In 2024, AGB_{fresh} decreased from 903 ± 521 g m^{-2} before grazing to 164 ± 88 g m^{-2} after grazing, while AGB_{dry} decreased from 406 ± 199 to 121 ± 51 g m^{-2}. In 2025, biomass levels were markedly higher, with AGB_{fresh} declining from 9143 ± 3074 to 3939 ± 1415 g m^{-2} and AGB_{dry} from 5992 ± 2231 to 2771 ± 1019 g m^{-2} between pre- and post-grazing conditions. In both years, differences between grazing phases were significant (one-way ANOVA, $p < 0.001$). These results show a strong interannual contrast between the two monitored seasons and a consistent reduction in both fresh and dry above-ground biomass after grazing.

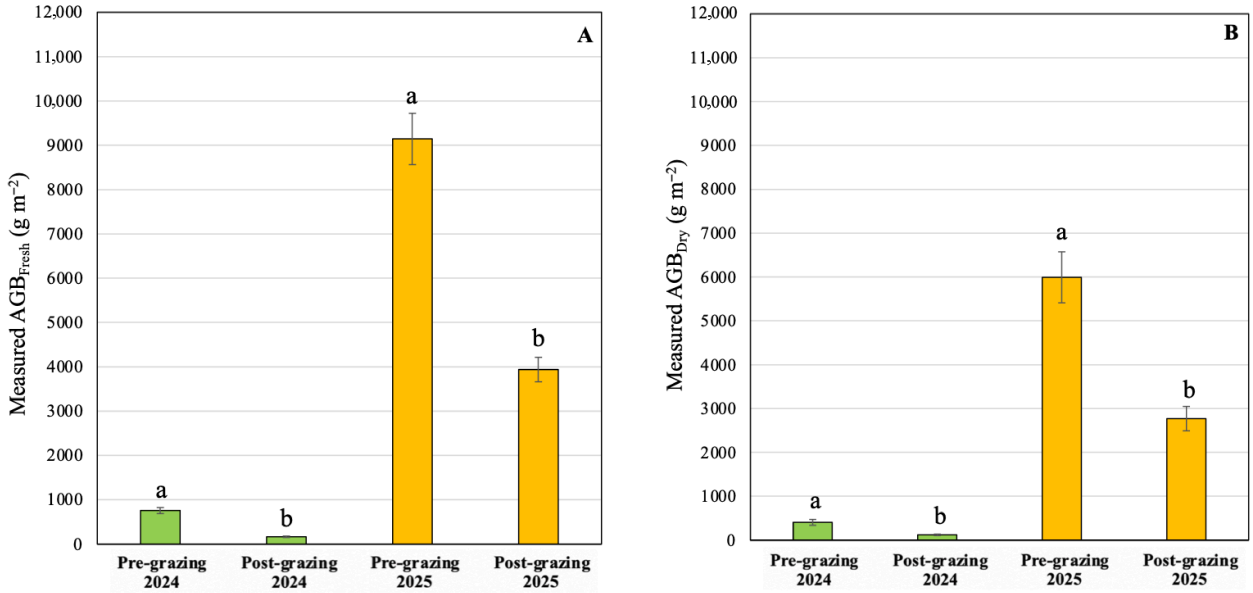

Figure 3. Fresh (**A**) and dry (**B**) mean above-ground biomass (AGB; g m^{-2}) measured under pre- and post-grazing conditions in 2024 and 2025. Different letters indicate significant differences between phases for each year and biomass variable ($p < 0.001$).

3.2. Calibration Performance of AGB Prediction Models

3.2.1. Model Calibration

After inter-sensor harmonization, calibration performances were more conservative than in the initial analysis, but they likely provide a more realistic estimate of model behavior across tests. The best calibration results were distributed across different VI families, including visible-band, soil-adjusted, red-edge, and atmosphere-resistant indices, rather than being restricted to a single group (Table 2).

For AGB_{fresh}, the highest calibration performances were obtained with GI, NGRDI, SAVI2, TSAVI, and MSRRE, with R^2 values ranging from 0.72 to 0.75 and RMSE values from 2063 to 2176 g m^{-2}. GI provided the best calibration performance for AGB_{fresh} (R^2 = 0.75; RMSE = 2063 g m^{-2}), followed by NGRDI and GRVI (R^2 = 0.74; RMSE = 2079 g m^{-2}), while SAVI2 and TSAVI showed comparable accuracy (R^2 = 0.73; RMSE = 2144 g m^{-2}), while MSRRE also provided good calibration performance (R^2 = 0.72; RMSE = 2176 g m^{-2}).

For AGB_{dry}, the best calibration performances were obtained with EVI2, SAVI2, TSAVI, NGRDI, GRVI, and GI, with R^2 values ranging from 0.71 to 0.75 and RMSE values from 1472 to 1517 g m^{-2} (Table 2). EVI2 showed the highest calibration (R^2 = 0.75; RMSE = 1517 g m^{-2}), whereas NGRDI and GRVI yielded the lowest RMSE (1472 g m^{-2}) with R^2 = 0.72. GI and SAVI2 also performed well, with R^2 values of 0.71–0.72 and RMSE values of 1486–1494 g m^{-2}.

Table 2. Regression models (equations) obtained between field-measured AGB_{fresh} and AGB_{dry} and the different vegetation indices (VIs). For each VI, the R^2 and RMSE (g m^{-2}) from the calibration models are reported.

Group	Index	AGB_{fresh} Calibration			AGB_{dry} Calibration		
		Equation	R^2	RMSE	Equation	R^2	RMSE
NIR–Red	**NDVI**	$42.052^{5.6836x}$	0.70	2370	$31.514^{5.416x}$	0.65	1800
	SR	281.43x + 833.68	0.65	2434	182.48x + 571.58	0.59	1766
	DVI	26,639x − 472.33	0.66	2396	17,333x − 121.43	0.67	1591
	IPVI	$11.982^{7.1232x}$	0.70	2313	$9.3544^{6.815x}$	0.65	1734
	MNDVI	$52.363^{5.6682x}$	0.68	2415	$39.08^{5.3905x}$	0.63	1826
NIR–Green	**GNDVI**	$12.589^{7.0668x}$	0.44	3370	$11.825^{6.4802x}$	0.39	2444
Contrast	**RDVI**	18,197x − 1706.6	0.67	2360	11,928x − 920	0.69	1549
	RTVI	277.1x + 3692.4	0.10	3875	124.22x + 2337.8	0.05	2706
	PVI	37,674x − 472.33	0.66	2396	24,512x − 121.43	0.67	1591
	WDRVI	7804.1x + 5512.3	0.69	2298	5100.9x + 3615.1	0.64	1664
Atmospherically resistant	**EVI**	14,077x − 781.3	0.64	2468	9138.8x − 285.95	0.66	1624
	EVI2	15,834x − 860.76	0.69	2295	$88.692^{5.7719x}$	0.75	1517
	ARVI2	$100.82^{4.8578x}$	0.70	2370	$72.506^{4.629x}$	0.65	1806
	GEMI	−50,358x + 49,972	0.08	3929	−16,524x + 21,359	0.01	2755
Soil-adjusted	**SAVI**	$173.34^{7.3189x}$	0.55	3705	$141.89^{6.9139x}$	0.56	2318
	SAVI2	$105.84^{6.0549x}$	0.73	2144	$88.692^{5.7719x}$	0.72	1486
	OSAVI	$128.71^{7.0046x}$	0.68	2485	$108.34^{6.6445x}$	0.68	1684
	MSAVI	91.249x + 137.27	0.23	5336	65.286x − 112.56	0.26	3698
	GOSAVI	$94.049^{7.7886x}$	0.69	2316	$86.017^{7.3434x}$	0.69	1556
	TSAVI	$105.84^{6.0549x}$	0.73	2144	$88.692^{5.7719x}$	0.72	1486
Red-edge/Chlorophyll	**NDRE**	$95.534^{5.6785x}$	0.67	2439	$68.958^{5.4087x}$	0.61	1826
	Cl_RE	91.249x + 137.27	0.23	5266	65.286x − 112.56	0.26	3698
	MSRRE	10,195x − 1502.7	0.72	2176	6714.1x − 995.29	0.68	1569
VIS	**NGRDI**	14,933x + 3787.8	0.74	2079	9937.9x + 2490.1	0.72	1472
	GLI	$311.74^{6.6752x}$	0.62	3017	$185.01^{6.9797x}$	0.58	2072
	GRVI	−14,933x + 3787.8	0.74	2079	−9937.9x + 2490.1	0.72	1472
	GI	5503.9x − 2577.4	0.75	2063	3631.8x − 1711	0.71	1494
	GCI	632.08x − 155.94	0.45	3042	402.67x − 27.445	0.4	2151
	CVI	−165.51x + 4713	0.02	4045	−133.73x + 3263.7	0.03	2723
Water/Pigment-stress	**NDWI**	$12.589^{-7.067x}$	0.44	3370	$11.825^{-6.48x}$	0.39	2444
	SIPI2	$16.733^{6.8005x}$	0.61	2763	$14.01^{6.3766x}$	0.56	2073
Triangular/Geometry-based	**TriVI**	475.35x − 858.27	0.70	2242	281.68x − 64.583	0.68	1570
	TVI	$0.0392^{8.2726x}$	0.68	2562	$0.043^{7.8422x}$	0.64	1940

Model calibration scatterplots for the selected indices are shown in Figures 4 and 5 for AGB_{fresh} and AGB_{dry}, respectively. In the calibration dataset, most high-performing soil-adjusted indices, including SAVI, OSAVI, GOSAVI, SAVI2 and TSAVI, were best described by exponential relationships for both AGB_{fresh} and AGB_{dry} (Table 2 and Figures 4 and 5).

In contrast, several visible-band greenness indices, including GI, NGRDI, GRVI, followed linear relationships while maintaining relatively high R^2 values.

Overall, visible-band greenness indices remained among the most competitive calibration predictors, whereas several conventional NIR-based indices showed only moderate performance. Contrast-based and red-edge/chlorophyll indices, such as RDVI and MSRRE, also provided relatively strong results, although they generally did not exceed the best visible-band formulations. In contrast, GEMI, RTVI, and CVI showed negligible explana-

tory power and high prediction errors and were therefore not considered further among the most informative predictors.

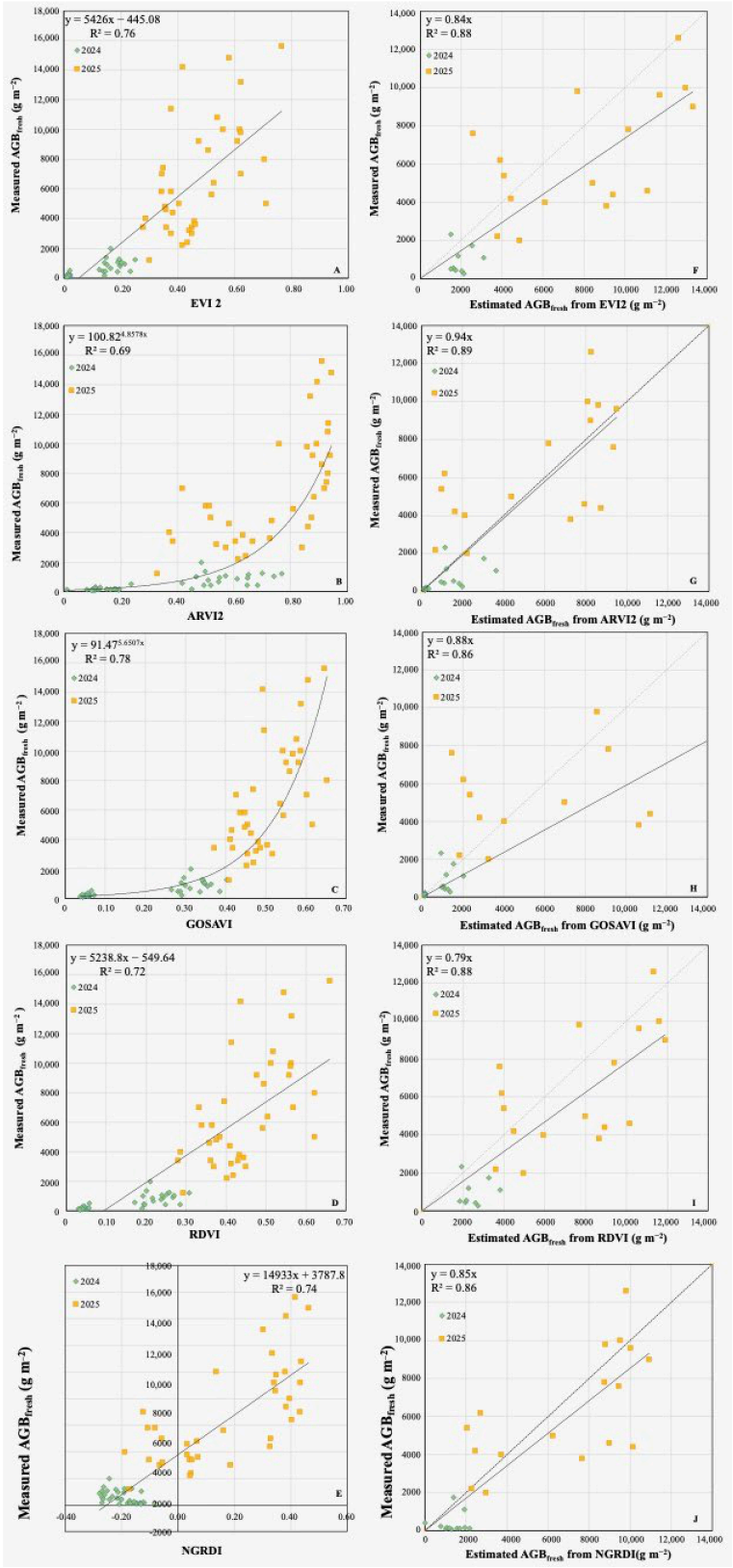

Figure 4. Model calibration (panels (**A**–**E**), measured AGB_{fresh} vs. VI) and validation scatterplots (panels (**F**–**J**), measured vs. predicted AGB_{fresh}) for the five selected indices in terms of AGB_{fresh}.

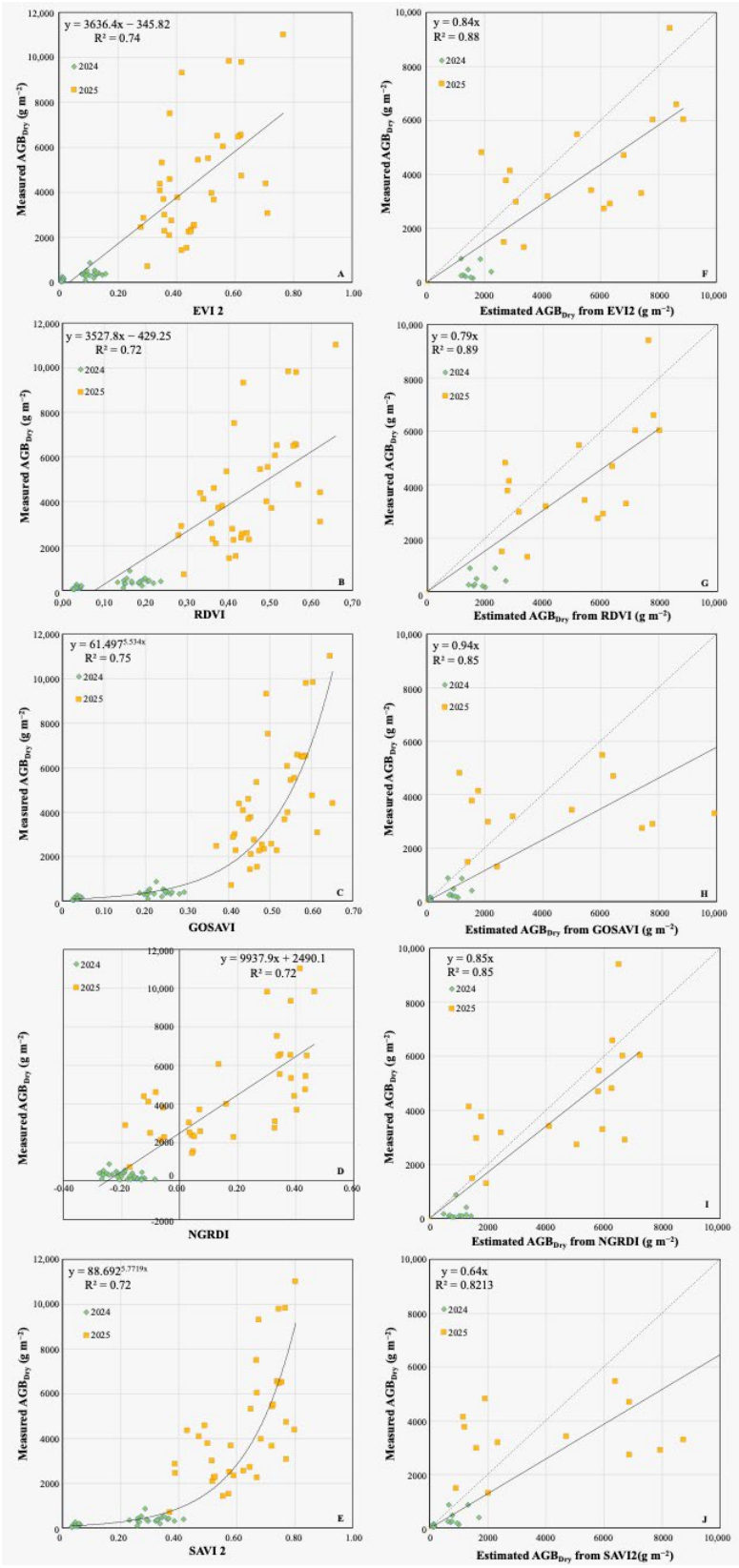

Figure 5. Model calibration (panels (**A**–**E**), measured AGB_{dry} vs. VI) and validation scatterplots (panels (**F**–**J**), measured vs. predicted AGB_{dry}) for the five selected indices in terms of AGB_{dry}.

In contrast, the NIR–green index GNDVI showed lower calibration accuracy than the best-performing indices, with R^2 = 0.44 and 0.38; RMSE values of 3383 and 2444 g m^{-2} for AGB_{fresh} and AGB_{dry}, respectively.

Red-edge/chlorophyll indices offered intermediate performances, with NDRE (exponential fit) and MSRRE (linear fit) yielding R^2 values of 0.67–0.72 and RMSE varying between 2176 and 2443 g m^{-2} for AGB_{fresh}, and R^2 values of 0.61–0.68 and RMSE ranging from 1570 to 1826 g m^{-2} for AGB_{dry} (Table 2). Indices showing near-zero explanatory power included GEMI, RTVI and CVI, which yielded $R^2 \leq 0.03$ in both AGB_{fresh} and AGB_{dry} (Table 2), with correspondingly high errors (e.g., RMSE = 4092–4095 g m^{-2} for AGB_{fresh} and 2723–2755 g m^{-2} for AGB_{dry}).

For example, Figure 6 shows the spatial representation of predicted AGB_{fresh} for the four monitoring dates, highlighting the reduction in biomass after grazing and the greater spatial heterogeneity under post-grazing conditions.

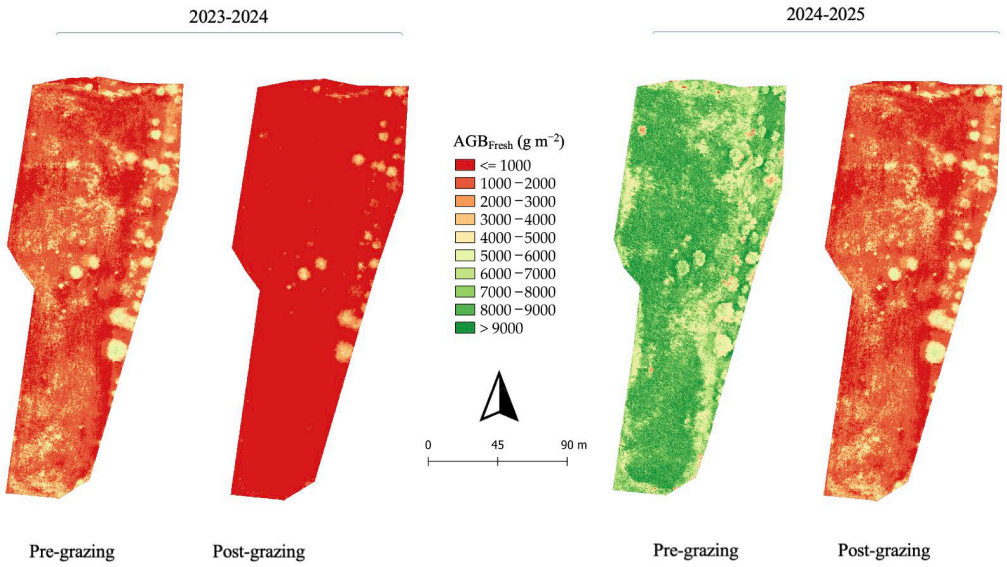

Figure 6. Spatial representation of predicted AGB_{fresh} for the four monitored dates under pre- and post-grazing conditions during 2024 and 2025. The figure illustrates the relative spatial distribution of biomass classes within the study pasture based on the ARVI2-derived modelling framework.

3.2.2. Model Validation

In the independent validation subset (33% hold-out), model performance showed patterns generally consistent with those observed during calibration (Section 3.2.1). Several visible-band, atmosphere-resistant, contrast-based, and soil-adjusted indices remain among the best AGB predictors in the pooled validation dataset (Table 3, Figure 7). Validation metrics were computed on the hold-out subset pooled across the 2024 and 2025 seasons, providing an overall assessment of model performance across contrasting biomass ranges.

For AGB_{fresh}, the highest validation R^2 values were obtained with EVI2 and ARVI2 (R^2 = 0.89), although ARVI2 provided a lower RMSE (2047 g m^{-2}) than EVI2 (2484 g m^{-2}) (Table 3, Figure 4). GOSAVI also showed high explanatory power (R^2 = 0.87), but with a markedly higher RMSE (3759 g m^{-2}), indicating lower predictive precision. Among the visible-band indices, NGRDI and GRVI were particularly competitive, with R^2 = 0.86 and RMSE = 2008 g m^{-2}, while GI showed a similar performance (R^2 = 0.86; RMSE = 2099 g m^{-2}).

For AGB_{dry}, validation accuracy remained high for several indices. EVI and EVI2 both reached R^2 = 0.86, with RMSE values of 1551 and 1662 g m^{-2}, respectively, whereas DVI and PVI reached R^2 = 0.87 but showed higher prediction errors (RMSE = 1838 g m^{-2}) (Table 3, Figure 5). Among the visible-band indices, NGRDI and GRVI showed one of the best overall performances, with R^2 = 0.85 and RMSE = 1371 g m^{-2}, while GI also remained stable (R^2 = 0.84; RMSE = 1432 g m^{-2}). RDVI provided a similar result in terms of explanatory

power (R^2 = 0.85), but with a higher RMSE (1565 g m^{-2}). Soil-adjusted indices showed moderate validation performance compared with the best visible-band and atmospherically resistant indices. SAVI2 and TSAVI reached R^2 = 0.82 and RMSE = 2143 g m^{-2} for AGB_{dry}, while GOSAVI reached R^2 = 0.82 and RMSE = 2578 g m^{-2}, and OSAVI reached R^2 = 0.80 and RMSE = 3388 g m^{-2}. For AGB_{fresh}, GOSAVI showed high R^2 (0.87), although with a relatively high RMSE (3759 g m^{-2}), whereas SAVI2 and TSAVI reached R^2 = 0.82 and RMSE = 3214 g m^{-2}.

Overall, validation results indicated that a limited group of visible-band, atmospherically resistant, and contrast-based indices provided the most robust biomass predictions across the pooled dataset (Table 3; Figure 7).

Table 3. Comparison between the AGB (AGB_{fresh} and AGB_{dry}) estimated from the developed models and the AGB values measured in the field. For each VI, the R^2 and RMSE (g m^{-2}) from the models' validation are reported.

Group		Fresh Validation			Dry Validation		
	Index	**Equation**	**R^2**	**RMSE**	**Equation**	**R^2**	**RMSE**
NIR–Red	**NDVI**	0.9619x	0.82	2047	1.0761x	0.80	1462
	SR	0.8599x	0.81	2253	0.8596x	0.78	1598
	DVI	0.6866x	0.85	2809	0.6866x	0.87	1838
	IPVI	0.8855x	0.82	2150	0.9876x	0.80	1462
	MNDVI	0.9474x	0.82	2119	1.0609x	0.79	1501
NIR–Green	**GNDVI**	1.2343x	0.70	2811	1.3878x	0.66	2044
Contrast	**RDVI**	0.7803x	0.86	2269	0.7627x	0.85	1565
	RTVI	0.8833x	0.55	3335	0.9376x	0.52	2280
	PVI	0.6866x	0.85	2809	0.6866x	0.87	1838
	WDRVI	0.8828x	0.83	2121	0.8472x	0.81	1537
Atmospherically resistant	**EVI**	0.7687x	0.86	2322	0.7594x	0.86	1551
	EVI2	0.8404x	0.89	2484	0.7287x	0.86	1662
	ARVI2	0.944x	0.89	2047	1.0762x	0.80	1462
	GEMI	−0.4231x	0.46	11,754	0.9066x	0.45	2438
Soil-adjusted	**SAVI**	0.2407x	0.70	13,265	0.2709x	0.74	7743
	SAVI2	0.6477x	0.82	3214	0.6447x	0.82	2143
	OSAVI	0.4752x	0.78	5333	0.4895x	0.80	3388
	MSAVI	188.86x	0.63	4796	126.81x	0.64	3325
	GOSAVI	0.8768x	0.87	3759	0.5771x	0.82	2578
	TSAVI	0.6477x	0.82	3214	0.6447x	0.82	2143
Red-edge/Chlorophyll	**NDRE**	0.9097x	0.82	2161	1.022x	0.80	1483
	Cl_RE	188.86x	0.63	4724	126.81x	0.64	3325
	MSRRE	0.8173x	0.83	2274	0.8111x	0.80	1621
VIS	**NGRDI**	0.853x	0.86	2008	0.8532x	0.85	1371
	GLI	1.1953x	0.78	2399	1.1547x	0.77	1610
	GRVI	0.853x	0.86	2008	0.8532x	0.85	1371
	GI	0.8306x	0.86	2099	0.8334x	0.84	1432
	GCI	0.8704x	0.71	2733	2.9346x	0.59	3483
	CVI	0.9512x	0.49	3527	0.9532x	0.48	2363
Water/Pigment-stress	**NDWI**	1.2341x	0.70	2811	1.388x	0.66	2045
	SIPI2	1.0746x	0.79	2288	1.2099x	0.76	1688
Triangular/Geometry-based	**TriVI**	0.6397x	0.84	3214	0.6796x	0.86	1875
	TVI	1.0953x	0.83	2066	1.2181x	0.80	1542

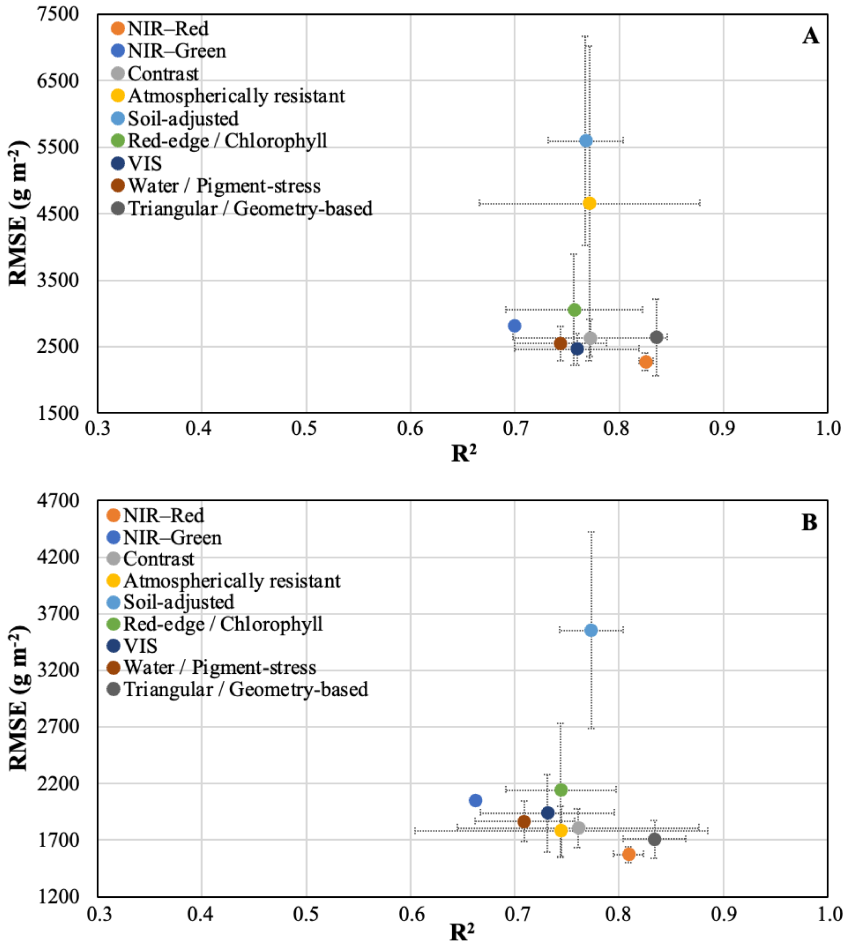

Figure 7. Correlation between R^2 and RMSE (g m^{-2}) obtained in the validation process for AGB_{fresh} (**A**) and AGB_{dry} (**B**). Metrics are computed on the 33% validation subset pooled across 2024 and 2025 (models trained on the 66% calibration set).

4. Discussion

The strong interannual contrast observed in ground-measured biomass highlights the sensitivity of Mediterranean pastures to seasonal rainfall distribution and water availability. The higher rainfall recorded during the 2024–2025 season, particularly during the autumn–early spring period, likely contributed to the markedly greater biomass values observed in 2025. This broader biomass range was useful for testing UAV-derived spectral relationships under contrasting pasture conditions, including both low-biomass post-grazing conditions and dense pre-grazing canopy cover.

After inter-sensor harmonization, calibration and validation performances were distributed across different vegetation-index families, including visible-band, soil-adjusted, red-edge/chlorophyll, atmospherically resistant, and contrast-based indices, rather than being restricted to a single group. This behavior indicates that soil-adjusted indices, explicitly developed to reduce the influence of soil brightness and background contributions in the red–NIR feature space, remain relevant under heterogeneous cover and partial exposure of bare soil, but that visible-band greenness indices may perform equally well or better under the observed pasture conditions [53]. Likewise, EVI2 was introduced to retain improved sensitivity relative to NDVI while avoiding the blue band, which supports stable performance in multispectral UAV workflows [50].

The validation results also showed that the best-performing index depended on the target biomass variable and on the balance between explained variance and prediction error. For AGB_{fresh}, ARVI2 combined the highest validation R^2 with a lower RMSE than

EVI2, whereas visible-band indices such as NGRDI, GRVI, and GI showed similarly strong and stable performance. For AGB_{dry}, NGRDI and GRVI provided the lowest validation RMSE, despite EVI, EVI2, DVI, and PVI reaching comparable or slightly higher R^2 values. Therefore, model selection should not be based only on R^2, but should also consider RMSE, especially when models are intended for operational biomass estimation.

The strong performance of visible-band greenness indices is particularly relevant from an operational perspective. These indices are simple to compute and rely on spectral regions that are commonly available across UAV sensors. Their competitive performance suggests that biomass variability in this pasture could be captured effectively even without relying exclusively on NIR-based combinations. In contrast, several conventional NIR-based indices showed only moderate performance, probably reflecting the combined influence of canopy density, soil exposure, and saturation effects across the wide biomass range considered in the study.

Additionally, other UAV-based pasture studies [70,71] reported that vegetation indices can provide reliable biomass estimates, although model robustness may be influenced by sward heterogeneity and background effects and may improve when spectral predictors are combined with UAV-derived structural metrics, such as sward height. In the present study, most high-performing soil-adjusted indices were best described by exponential relationships for both AGB_{fresh} and AGB_{dry}. This pattern is consistent with a progressive loss of sensitivity at higher canopy densities. Specifically, exponential models capture a rapid response at low–intermediate biomass followed by a flattening at high VI values, whereas linear models imply a more uniform sensitivity across the observed range [49,56].

From an ecological perspective, the observed model behaviour is consistent with the structural and management characteristics of the study pasture [54]. Grazing reduced canopy biomass and increased the exposure of soil and shadowed background elements, especially under post-grazing conditions, thereby increasing spectral heterogeneity within the field [72]. Under these conditions, indices based on visible-band greenness and soil-adjusted formulations may retain good sensitivity because they respond not only to canopy vigour but also to changes in background contrast and partial cover [45,68]. Comparable background effects on VI performance have been documented in rangeland studies, where OSAVI offered more reliable biomass/cover estimates than NDVI under sparse vegetation and high soil exposure [73]. UAV-based grazing experiments also reported that increased soil background after grazing altered spectral responses and can potentially limit the sensitivity of traditional indices, supporting the use of approaches that reduce background influence [74].

In addition, the marked biomass differences between the two monitored growing seasons suggest that canopy density and vertical structure also influenced index performance, with denser and more productive conditions likely increasing the risk of saturation for some conventional NIR-based indices. These ecological and structural factors help explain why no single index was universally superior across all conditions and why a small group of robust indices performed more consistently across seasons and grazing phases.

Overall, these findings support the selection of a small set of operationally useful candidate indices rather than a single universally superior predictor. This is important for practical pasture monitoring because index selection may need to be adapted to the target biomass variable, sensor configuration, and management objective. The proposed workflow has the advantage of being simple, interpretable, and compatible with routine UAV acquisitions. Compared with approaches based on multiple predictors, structural metrics, or machine-learning algorithms, single-index empirical models require fewer input variables and are easier to interpret at the farm scale. However, this simplicity also involves some limitations. Broader validation across additional sites, seasons, pasture types, and

grazing intensities is required to strengthen model transferability. Although inter-sensor harmonization was applied, the use of two different UAV multispectral systems may still introduce residual uncertainty. Future studies should therefore assess whether lightweight multivariate approaches, structural descriptors, or environmental covariates can improve prediction reliability without compromising operational simplicity.

5. Conclusions

This study demonstrated that multispectral UAV imagery can provide a promising and interpretable approach for estimating fresh and dry above-ground biomass (AGB_{fresh} and AGB_{dry}, respectively) in a semi-arid Mediterranean *Hedysarum coronarium* ("Sulla") pasture managed under rotational grazing using a simple single-index approach. Validation on an independent hold-out subset confirmed good model performance across contrasting grazing phases and growing seasons, with several indices showing competitive results rather than a single universally superior predictor. In particular, EVI2, RDVI, GOSAVI, NGRDI, and GI emerged among the most reliable candidates, depending on the target biomass variable and the balance between explained variance and prediction error.

Strengths of the proposed workflow include low computational complexity, interpretability, and ease of replication with routine UAV flights, making it suitable for farm-scale monitoring and spatial decision support. Compared with studies that integrate structural descriptors, multiple predictors, or machine-learning approaches, the present study prioritizes operational simplicity and transparency while still delivering good predictive performance.

Limitations include non-negligible absolute prediction errors across the widest biomass ranges, sensitivity to soil/shadow/background effects under post-grazing heterogeneity, and potential saturation at high canopy density.

In addition, model comparison was restricted to single-index linear and exponential regressions. Although this choice was consistent with the objective of testing a simple and interpretable UAV-based workflow, alternative multivariate approaches such as multiple linear regression may capture complementary information and should be assessed in future research based on broader datasets. A further limitation is the relatively limited sample size in relation to the number of evaluated vegetation indices, despite the use of simple single-predictor models and independent validation. Although the results were consistent enough to identify a restricted group of robust candidate indices, broader datasets covering more dates, seasons, pasture types, and environmental conditions will be necessary to strengthen model stability, transferability, and generalizability.

Future work should test the robustness of the proposed approach across additional Mediterranean pasture systems and evaluate whether combining spectral indices with lightweight structural information, environmental covariates, or multivariate modelling strategies can improve prediction reliability without compromising field applicability and interpretability.

Supplementary Materials: The following supporting information can be downloaded at https://www.mdpi.com/article/10.3390/rs18101594/s1. Figure S1: Cross-sensor radiometric calibration between MicaSense RedEdge-MX and DJI Phantom 4 Multispectral bands. Relationship between band reflectance values extracted from the two sensors (p_M3M vs. p_ALTUM) for the NIR, RedEdge, Green, and Red bands. The dashed yellow line represents the fitted linear regression used to harmonize the datasets acquired in different years; the equation and coefficient of determination (R2) are reported in the figure. Table S1: Summary of the vegetation indices identified in the scientific articles included in the present review and the formula for their calculation.

Author Contributions: Conceptualization, J.M.R.-C., N.F. and S.I.G.F.; methodology, J.M.R.-C., N.F. and S.I.G.F.; formal analysis, G.S., J.M.R.-C., N.F. and S.I.G.F.; investigation, N.F.; data curation, N.F.; writing—original draft preparation, N.F.; writing—review and editing, J.M.R.-C. and S.I.G.F.; supervision, M.A., M.B., L.B., J.M.R.-C. and S.I.G.F.; funding acquisition, S.I.G.F. and L.B. All authors have read and agreed to the published version of the manuscript.

Funding: This research was funded by the European Union—NextGenerationEU, through Italy's National Recovery and Resilience Plan (PNRR), Mission 4, Component 2, Investment 1.4, "National Research Center for Agricultural Technologies (Agritech)" (Spoke 5, Task 5.3.1), under the Recovery and Resilience Facility (RRF); and by "Gen.Al.Tec." project—Line 1, University Research Incentive Plan 2024/2026, P.I. Prof. Andrea Criscione.

Data Availability Statement: Dataset available on request from the authors.

Acknowledgments: The authors would thank the European Union—Next-GenerationEU—National Recovery and Resilience Plan (NRRP)—MISSION 4 COMPONENT 2, INVESTIMENT N. 1.4, "National Research Centre for Agricultural Technologies" (Agritech—Spoke 5 Task 5.3.1), integrated within the scope of the Recovery and Resilience Mechanism (RRM) of the European Union (EU), for supporting the research. They also thank the "Gen.Al.Tec." project—Line 1, University Research Incentive Plan 2024/2026, P.I. Andrea Criscione. J.M. Ramírez-Cuesta gratefully acknowledges the postdoctoral contract from the 'Ramón y Cajal' programme (RYC-2023-045589), supplied by the Spanish Ministry of Economy, Industry and Competitiveness (MINECO).

Conflicts of Interest: The authors declare no conflicts of interest. The funders had no role in the design of the study; in the collection, analyses, or interpretation of data; in the writing of the manuscript; or in the decision to publish the results.

References

1. Suttie, J.M.; Reynolds, S.G.; Batello, C. (Eds.) *Grasslands of the World*; Food and Agriculture Organization of the United Nations: Rome, Italy, 2005; Volume 34.
2. Peeters, A. Importance, Evolution, Environmental Impact and Future Challenges of Grasslands and Grassland-based Systems in Europe. *Grassl. Sci.* **2009**, *55*, 113–125. [CrossRef]
3. Soussana, J.; Lüscher, A. Temperate Grasslands and Global Atmospheric Change: A Review. *Grass Forage Sci.* **2007**, *62*, 127–134. [CrossRef]
4. Lemaire, G.; Hodgson, J.; Chabbi, A. (Eds.) *Grassland Productivity and Ecosystem Services*, 1st ed.; CABI: Wallingford, UK, 2011.
5. Soussana, J.F.; Tallec, T.; Blanfort, V. Mitigating the Greenhouse Gas Balance of Ruminant Production Systems through Carbon Sequestration in Grasslands. *Animal* **2010**, *4*, 334–350. [CrossRef] [PubMed]
6. Sangjan, W.; McGee, R.J.; Sankaran, S. Optimization of UAV-Based Imaging and Image Processing Orthomosaic and Point Cloud Approaches for Estimating Biomass in a Forage Crop. *Remote Sens.* **2022**, *14*, 2396. [CrossRef]
7. Wilkinson, J.M.; Lee, M.R.F.; Rivero, M.J.; Chamberlain, A.T. Some Challenges and Opportunities for Grazing Dairy Cows on Temperate Pastures. *Grass Forage Sci.* **2020**, *75*, 1–17. [CrossRef] [PubMed]
8. Reinermann, S.; Gessner, U.; Asam, S.; Ullmann, T.; Schucknecht, A.; Kuenzer, C. Detection of Grassland Mowing Events for Germany by Combining Sentinel-1 and Sentinel-2 Time Series. *Remote Sens.* **2022**, *14*, 1647. [CrossRef]
9. Furnitto, N.; Ramírez-Cuesta, J.M.; Intrigliolo, D.S.; Todde, G.; Failla, S. Remote Sensing for Pasture Biomass Quantity and Quality Assessment: Challenges and Future Prospects. *Smart Agric. Technol.* **2025**, *12*, 101057. [CrossRef]
10. Koc, A.B.; MacInnis, B.M.; Aguerre, M.J.; Chastain, J.P.; Turner, A.P. Alfalfa Biomass Estimation Using Crop Surface Modeling and NDVI. *Appl. Eng. Agric.* **2023**, *39*, 251–264. [CrossRef]
11. Hatfield, J.L.; Gitelson, A.A.; Schepers, J.S.; Walthall, C.L. Application of Spectral Remote Sensing for Agronomic Decisions. *Agron. J.* **2008**, *100*, S-117. [CrossRef]
12. Cooper, S.; Roy, D.; Schaaf, C.; Paynter, I. Examination of the Potential of Terrestrial Laser Scanning and Structure-from-Motion Photogrammetry for Rapid Nondestructive Field Measurement of Grass Biomass. *Remote Sens.* **2017**, *9*, 531. [CrossRef]
13. Rahali, L.; Praticò, S.; Lanucara, S.; Modica, G. CubeSat Constellations: New Era for Precision Agriculture? *Comput. Electron. Agric.* **2025**, *230*, 109764. [CrossRef]
14. Rahali, L.; Praticò, S.; Messina, G.; Lanucara, S.; Modica, G. Assessing the Efficacy of PlanetScope SuperDove Multispectral Data in Citrus Orchard Management: Preliminary Results. In *Proceedings of the International Mid-Term Conference of the Italian Association of Agricultural Engineering*; Springer Nature: Cham, Switzerland, 2024; pp. 649–656.

15. Wang, J.; Xiao, X.; Bajgain, R.; Starks, P.; Steiner, J.; Doughty, R.B.; Chang, Q. Estimating Leaf Area Index and Aboveground Biomass of Grazing Pastures Using Sentinel-1, Sentinel-2 and Landsat Images. *ISPRS J. Photogramm. Remote Sens.* **2019**, *154*, 189–201. [CrossRef]
16. Chen, Y.; Guerschman, J.; Shendryk, Y.; Henry, D.; Harrison, M.T. Estimating Pasture Biomass Using Sentinel-2 Imagery and Machine Learning. *Remote Sens.* **2021**, *13*, 603. [CrossRef]
17. Peng, J.; Zeiner, N.; Parsons, D.; Féret, J.-B.; Söderström, M.; Morel, J. Forage Biomass Estimation Using Sentinel-2 Imagery at High Latitudes. *Remote Sens.* **2023**, *15*, 2350. [CrossRef]
18. Adar, S.; Sternberg, M.; Paz-Kagan, T.; Henkin, Z.; Dovrat, G.; Zaady, E.; Argaman, E. Estimation of Aboveground Biomass Production Using an Unmanned Aerial Vehicle (UAV) and VENμS Satellite Imagery in Mediterranean and Semiarid Rangelands. *Remote Sens. Appl. Soc. Environ.* **2022**, *26*, 100753. [CrossRef]
19. Verrelst, J.; Camps-Valls, G.; Muñoz-Marí, J.; Rivera, J.P.; Veroustraete, F.; Clevers, J.G.P.W.; Moreno, J. Optical Remote Sensing and the Retrieval of Terrestrial Vegetation Bio-Geophysical Properties—A Review. *ISPRS J. Photogramm. Remote Sens.* **2015**, *108*, 273–290. [CrossRef]
20. Furnitto, N.; Ramírez-Cuesta, J.M.; Sottosanti, G.; Schillaci, G.; Failla, S.I.G. Appraising the Use of Remote and Proximal Platforms for Wheat Biomass Estimation from Multispectral Imagery. In *Biosystems Engineering Promoting Resilience to Climate Change—AIIA 2024—Mid-Term Conference*; Sartori, L., Tarolli, P., Guerrini, L., Zuecco, G., Pezzuolo, A., Eds.; Lecture Notes in Civil Engineering; Springer Nature: Cham, Switzerland, 2025; Volume 586, pp. 664–671.
21. Delegido, J.; Verrelst, J.; Alonso, L.; Moreno, J. Evaluation of Sentinel-2 Red-Edge Bands for Empirical Estimation of Green LAI and Chlorophyll Content. *Sensors* **2011**, *11*, 7063–7081. [CrossRef] [PubMed]
22. Rivera, J.; Verrelst, J.; Delegido, J.; Veroustraete, F.; Moreno, J. On the Semi-Automatic Retrieval of Biophysical Parameters Based on Spectral Index Optimization. *Remote Sens.* **2014**, *6*, 4927–4951. [CrossRef]
23. Corti, M.; Cavalli, D.; Cabassi, G.; Bechini, L.; Pricca, N.; Paolo, D.; Marinoni, L.; Vigoni, A.; Degano, L.; Marino Gallina, P. Improved Estimation of Herbaceous Crop Aboveground Biomass Using UAV-Derived Crop Height Combined with Vegetation Indices. *Precis. Agric.* **2023**, *24*, 587–606. [CrossRef]
24. Mutanga, O.; Skidmore, A.K. Narrow Band Vegetation Indices Overcome the Saturation Problem in Biomass Estimation. *Int. J. Remote Sens.* **2004**, *25*, 3999–4014. [CrossRef]
25. Gitelson, A.A.; Viña, A.; Verma, S.B.; Rundquist, D.C.; Arkebauer, T.J.; Keydan, G.; Leavitt, B.; Ciganda, V.; Burba, G.G.; Suyker, A.E. Relationship between Gross Primary Production and Chlorophyll Content in Crops: Implications for the Synoptic Monitoring of Vegetation Productivity. *J. Geophys. Res.* **2006**, *111*, 2005JD006017. [CrossRef]
26. Glenn, E.P.; Huete, A.R.; Nagler, P.L.; Nelson, S.G. Relationship Between Remotely-Sensed Vegetation Indices, Canopy Attributes and Plant Physiological Processes: What Vegetation Indices Can and Cannot Tell Us About the Landscape. *Sensors* **2008**, *8*, 2136–2160. [CrossRef] [PubMed]
27. Furnitto, N.; Ramírez-Cuesta, J.M.; Sottosanti, G.; Longo, D.; Schillaci, G.; Failla, S. Potentiality of Multispectral Vegetation Indexes for Evaluating the Influence of the Sowing Technique on Durum Wheat Cultivation Density. In *Safety, Health and Welfare in Agriculture and Agro-Food Systems*; Berruto, R., Biocca, M., Cavallo, E., Cecchini, M., Failla, S., Romano, E., Eds.; Lecture Notes in Civil Engineering; Springer Nature: Cham, Switzerland, 2024; Volume 521, pp. 313–321.
28. Calcagno, F.; Romano, E.; Furnitto, N.; Jamali, A.; Failla, S. Remote Sensing Monitoring of Durum Wheat under No Tillage Practices by Means of Spectral Indices Interpretation: A Preliminary Study. *Sustainability* **2022**, *14*, 15012. [CrossRef]
29. Romano, E.; Calcagno, F.; Bisaglia, C.; Furnitto, N.; Schillaci, G.; Failla, S. Application of Spectral Indices for the Evaluation of Conservative Techniques in Crops Management. In *AIIA 2022: Biosystems Engineering Towards the Green Deal*; Ferro, V., Giordano, G., Orlando, S., Vallone, M., Cascone, G., Porto, S.M.C., Eds.; Lecture Notes in Civil Engineering; Springer International Publishing: Cham, Switzerland, 2023; Volume 337, pp. 871–879.
30. Furnitto, N.; Failla, S.; Sottosanti, G.; Avondo, M.; Bognanno, M.; Ramirez-Cuesta, J.M. Can Remote Sensing Technologies Be Suitable for Monitoring and Estimating "Sulla" Grazing? In *Proceedings of the 2024 IEEE International Workshop on Metrology for Agriculture and Forestry (MetroAgriFor)*; IEEE: Padua, Italy, 2024; pp. 129–133.
31. Borra-Serrano, I.; De Swaef, T.; Muylle, H.; Nuyttens, D.; Vangeyte, J.; Mertens, K.; Saeys, W.; Somers, B.; Roldán-Ruiz, I.; Lootens, P. Canopy Height Measurements and Non-destructive Biomass Estimation of Lolium Perenne Swards Using UAV Imagery. *Grass Forage Sci.* **2019**, *74*, 356–369. [CrossRef]
32. Sinde-González, I.; Gil-Docampo, M.; Arza-García, M.; Grefa-Sánchez, J.; Yánez-Simba, D.; Pérez-Guerrero, P.; Abril-Porras, V. Biomass Estimation of Pasture Plots with Multitemporal UAV-Based Photogrammetric Surveys. *Int. J. Appl. Earth Obs. Geoinf.* **2021**, *101*, 102355. [CrossRef]
33. Lussem, U.; Bolten, A.; Menne, J.; Gnyp, M.L.; Schellberg, J.; Bareth, G. Estimating Biomass in Temperate Grassland with High Resolution Canopy Surface Models from UAV-Based RGB Images and Vegetation Indices. *J. Appl. Rem. Sens.* **2019**, *13*, 1. [CrossRef]

34. Dusseux, P.; Guyet, T.; Pattier, P.; Barbier, V.; Nicolas, H. Monitoring of Grassland Productivity Using Sentinel-2 Remote Sensing Data. *Int. J. Appl. Earth Obs. Geoinf.* **2022**, *111*, 102843. [CrossRef]
35. Adar, S.; Paz-Kagan, T.; Argaman, E.; Dubinin, M.; Sternberg, M. Identifying Climatic Drivers of Forage Quantity and Quality in Mediterranean Rangelands Using Remote Sensing. *Sci. Total Environ.* **2024**, *957*, 177797. [CrossRef]
36. MacTaggart, D.; Shirtliffe, S.; Beattie, A.; Lardner, H.A.; Biligetu, B. Application of a Multi-Spectral UAV Imagery in Germplasm Characterization: Prediction of Forage Biomass and Growth Patterns of Cicer Milkvetch (*Astragalus cicer* L.) Populations. *Agriculture* **2024**, *14*, 1969. [CrossRef]
37. Regione Siciliana; S.I.T.R.—Sistema Informativo Territoriale Regionale. *Carta dei Suoli Della Regione Siciliana, Edizione 1994, Scala 1:250.000 [Dataset/Online Map]*; Assessorato Regionale del Territorio e dell'Ambiente: Palermo, Italy, 2020; Available online: https://www.sitr.regione.sicilia.it/carta-dei-suoli-125-000/ (accessed on 5 January 2026).
38. Köppen Climate Classification. Encyclopaedia Britannica. Available online: https://www.britannica.com/science/Koppen-climate-classification/World-distribution-of-major-climatic-types (accessed on 15 October 2025).
39. Rouse, J.W., Jr.; Haas, R.H.; Schell, J.A.; Deering, D.W. Monitoring vegetation systems in the Great Plains with ERTS. In Proceedings of the Third Earth Resources Technology Satellite-1 Symposium, Washington, DC, USA, 10–14 December 1973; Volume 1, pp. 309–317.
40. Jordan, C.F. Derivation of leaf-area index from quality of light on the forest floor. *Ecology* **1969**, *50*, 663–666. [CrossRef]
41. Tucker, C.J. Red and photographic infrared linear combinations for monitoring vegetation. *Remote Sens. Environ.* **1979**, *8*, 127–150. [CrossRef]
42. Jackson, R.D.; Huete, A.R. Interpreting vegetation indices. *Prev. Vet. Med.* **1991**, *11*, 185–200. [CrossRef]
43. Vescovo, L.; Gianelle, D. Using the MIR bands in vegetation indices for the estimation of grassland biophysical parameters from satellite remote sensing in the Alps region of Trentino (Italy). *Adv. Space Res.* **2008**, *41*, 1764–1772. [CrossRef]
44. Gitelson, A.A.; Merzlyak, M.N. Signature analysis of leaf reflectance spectra: Algorithm development for remote sensing of chlorophyll. *J. Plant Physiol.* **1996**, *148*, 494–500. [CrossRef]
45. Roujean, J.-L.; Bréon, F.-M. Estimating PAR absorbed by vegetation from bidirectional reflectance measurements. *Remote Sens. Environ.* **1995**, *51*, 375–384. [CrossRef]
46. Haboudane, D.; Miller, J.R.; Pattey, E.; Zarco-Tejada, P.J.; Strachan, I.B. Hyperspectral vegetation indices and novel algorithms for predicting green LAI of crop canopies: Modeling and validation in the context of precision agriculture. *Remote Sens. Environ.* **2004**, *90*, 337–352. [CrossRef]
47. Lentile, L.B.; Holden, Z.A.; Smith, A.M.S.; Falkowski, M.J.; Hudak, A.T.; Morgan, P.; Lewis, S.A.; Gessler, P.E.; Benson, N.C. Remote sensing techniques to assess active fire characteristics and post-fire effects. *Int. J. Wildland Fire* **2006**, *15*, 319–345. [CrossRef]
48. Gitelson, A.A. Wide dynamic range vegetation index for remote quantification of biophysical characteristics of vegetation. *J. Plant Physiol.* **2004**, *161*, 165–173. [CrossRef] [PubMed]
49. Huete, A.; Didan, K.; Miura, T.; Rodriguez, E.P.; Gao, X.; Ferreira, L.G. Overview of the radiometric and biophysical performance of the MODIS vegetation indices. *Remote Sens. Environ.* **2002**, *83*, 195–213. [CrossRef]
50. Jiang, Z.; Huete, A.R.; Didan, K.; Miura, T. Development of a two-band enhanced vegetation index without a blue band. *Remote Sens. Environ.* **2008**, *112*, 3833–3845. [CrossRef]
51. Kaufman, Y.J.; Tanré, D. Atmospherically resistant vegetation index (ARVI) for EOS-MODIS. *IEEE Trans. Geosci. Remote Sens.* **1992**, *30*, 261–270. [CrossRef]
52. Pinty, B.; Verstraete, M.M. GEMI: A non-linear index to monitor global vegetation from satellites. *Vegetatio* **1992**, *101*, 15–20. [CrossRef]
53. Huete, A.R. A soil-adjusted vegetation index (SAVI). *Remote Sens. Environ.* **1988**, *25*, 295–309. [CrossRef]
54. Rondeaux, G.; Steven, M.; Baret, F. Optimization of soil-adjusted vegetation indices. *Remote Sens. Environ.* **1996**, *55*, 95–107. [CrossRef]
55. Qi, J.; Chehbouni, A.; Huete, A.R.; Kerr, Y.H.; Sorooshian, S. A modified soil-adjusted vegetation index. *Remote Sens. Environ.* **1994**, *48*, 119–126. [CrossRef]
56. Baret, F.; Guyot, G. Potentials and limits of vegetation indices for LAI and APAR assessment. *Remote Sens. Environ.* **1991**, *35*, 161–173. [CrossRef]
57. Gitelson, A.A.; Keydan, G.P.; Merzlyak, M.N. Three-band model for noninvasive estimation of chlorophyll, carotenoids, and anthocyanin contents in higher plant leaves. *Geophys. Res. Lett.* **2006**, *33*, L11402. [CrossRef]
58. Wang, R.; Dong, J.; Jin, L.; Sun, Y.; Baoyin, T.; Wang, X. Improving the accuracy of vegetation index retrieval for biomass by combining ground-UAV hyperspectral data: A new method for Inner Mongolia typical grasslands. *Phyton* **2024**, *93*, 387–411. [CrossRef]
59. Chen, J.M. Evaluation of vegetation indices and a modified simple ratio for boreal applications. *Can. J. Remote Sens.* **1996**, *22*, 229–242. [CrossRef]

60. Gitelson, A.A.; Kaufman, Y.J.; Stark, R.; Rundquist, D. Novel algorithms for remote estimation of vegetation fraction. *Remote Sens. Environ.* **2002**, *80*, 76–87. [CrossRef]
61. Louhaichi, M.; Borman, M.M.; Johnson, D.E. Spatially located platform and aerial photography for documentation of grazing impacts on wheat. *Geocarto Int.* **2001**, *16*, 65–70. [CrossRef]
62. Zha, Y.; Gao, J.; Ni, S. Use of normalized difference built-up index in automatically mapping urban areas from TM imagery. *Int. J. Remote Sens.* **2003**, *24*, 583–594. [CrossRef]
63. Smith, R.C.G.; Adams, J.; Stephens, D.J.; Hick, P.T. Forecasting wheat yield in a Mediterranean-type environment from the NOAA satellite. *Aust. J. Agric. Res.* **1995**, *46*, 113–125. [CrossRef]
64. Gitelson, A.A.; Merzlyak, M.N. Remote sensing of chlorophyll concentration in higher plant leaves. *Adv. Space Res.* **1998**, *22*, 689–692. [CrossRef]
65. Hunt, E.R., Jr.; Daughtry, C.S.T.; Eitel, J.U.H.; Long, D.S. Remote sensing leaf chlorophyll content using a visible band index. *Agron. J.* **2011**, *103*, 1090–1099. [CrossRef]
66. McFeeters, S.K. The use of the normalized difference water index (NDWI) in the delineation of open water features. *Int. J. Remote Sens.* **1996**, *17*, 1425–1432. [CrossRef]
67. Peñuelas, J.; Baret, F.; Filella, I. Semi-empirical indices to assess carotenoids/chlorophyll a ratio from leaf spectral reflectance. *Photosynthetica* **1995**, *31*, 221–230.
68. Broge, N.H.; Leblanc, E. Comparing prediction power and stability of broadband and hyperspectral vegetation indices for estimation of green leaf area index and canopy chlorophyll density. *Remote Sens. Environ.* **2001**, *76*, 156–172. [CrossRef]
69. Perry, C.R.; Lautenschlager, L.F. Functional equivalence of spectral vegetation indices. *Remote Sens. Environ.* **1984**, *14*, 169–182. [CrossRef]
70. Théau, J.; Lauzier-Hudon, É.; Aubé, L.; Devillers, N. Estimation of Forage Biomass and Vegetation Cover in Grasslands Using UAV Imagery. *PLoS ONE* **2021**, *16*, e0245784. [CrossRef]
71. Michez, A.; Lejeune, P.; Bauwens, S.; Herinaina, A.; Blaise, Y.; Castro Muñoz, E.; Lebeau, F.; Bindelle, J. Mapping and Monitoring of Biomass and Grazing in Pasture with an Unmanned Aerial System. *Remote Sens.* **2019**, *11*, 473. [CrossRef]
72. Li, J.; Wu, W.; Zhao, C.; Bai, X.; Dong, L.; Tan, Y.; Yusup, M.; Akelebai, G.; Dong, H.; Zhi, J. Effects of Solar Elevation Angle on the Visible Light Vegetation Index of a Cotton Field When Extracted from the UAV. *Sci. Rep.* **2025**, *15*, 18497. [CrossRef] [PubMed]
73. Fern, R.R.; Foxley, E.A.; Bruno, A.; Morrison, M.L. Suitability of NDVI and OSAVI as Estimators of Green Biomass and Coverage in a Semi-Arid Rangeland. *Ecol. Indic.* **2018**, *94*, 16–21. [CrossRef]
74. Guan, Q.; Jiang, M.; Du, W.; Chen, X.; Yan, B. Integrating UAV Visible and Multispectral Imagery to Assess Grazing-Induced Vegetation Responses in Sandy Grasslands. *Front. Plant Sci.* **2025**, *16*, 1730583. [CrossRef] [PubMed]